

Tunable ultrafast extreme ultraviolet source for time- and angle-resolved photoemission spectroscopy

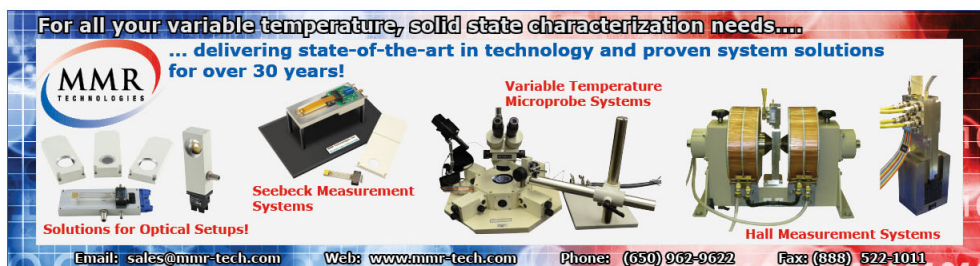
G. L. Dakovski, Y. Li, T. Durakiewicz, and G. Rodriguez

Citation: [Review of Scientific Instruments](#) **81**, 073108 (2010); doi: 10.1063/1.3460267

View online: <http://dx.doi.org/10.1063/1.3460267>

View Table of Contents: <http://scitation.aip.org/content/aip/journal/rsi/81/7?ver=pdfcov>

Published by the [AIP Publishing](#)

An advertisement for MMR Technologies. At the top, it says 'For all your variable temperature, solid state characterization needs....' and '... delivering state-of-the-art in technology and proven system solutions for over 30 years!'. Below this is the MMR Technologies logo. The advertisement features four images of scientific equipment: a 'Seebeck Measurement System' (a small electronic device), 'Variable Temperature Microprobe Systems' (a microscope with a probe), 'Hall Measurement Systems' (a large, complex machine with multiple coils), and 'Solutions for Optical Setups!' (a smaller optical device). At the bottom, contact information is provided: Email: sales@mmr-tech.com, Web: www.mmr-tech.com, Phone: (650) 962-9622, and Fax: (888) 522-1011.

Tunable ultrafast extreme ultraviolet source for time- and angle-resolved photoemission spectroscopy

G. L. Dakovski,¹ Y. Li,² T. Durakiewicz,² and G. Rodriguez¹

¹MPA-CINT, Los Alamos National Laboratory, Los Alamos, New Mexico 87545, USA

²MPA-CMMS, Los Alamos National Laboratory, Los Alamos, New Mexico 87545, USA

(Received 6 May 2010; accepted 14 June 2010; published online 20 July 2010)

We present a laser-based apparatus suitable for visible pump/extreme UV (XUV) probe time-, energy-, and angle-resolved photoemission spectroscopy utilizing high-harmonic generation from a noble gas. Tunability in a wide range of energies (currently 20–36 eV) is achieved by using a time-delay compensated monochromator, which also preserves the ultrashort duration of the XUV pulses. Using an amplified laser system at 10 kHz repetition rate, approximately 10^9 – 10^{10} photons/s per harmonic are made available for photoelectron spectroscopy. Parallel energy and momentum detection is carried out in a hemispherical electron analyzer coupled with an imaging detector. First applications demonstrate the capabilities of the instrument to easily select the probe wavelength of choice, to obtain angle-resolved photoemission maps (GaAs and URu₂Si₂), and to trace ultrafast electron dynamics in an optically excited semiconductor (Ge). © 2010 American Institute of Physics. [doi:10.1063/1.3460267]

I. INTRODUCTION

Angle-resolved photoemission spectroscopy (ARPES) is a well-established experimental technique for studying the electronic structure of solids.^{1,2} The simultaneous detection of the kinetic energy and angle of the emitted photoelectrons offers the possibility of obtaining a two-dimensional energy-momentum map along a given direction in *k*-space, thus providing accurate information about the dispersion of filled electronic bands. In principle ARPES can also be used to map out the dispersion of normally unoccupied bands provided that electrons are excited (“pumped”) into unfilled bands and subsequently photoemitted (“probed”). The dynamics of the transient electrons is typically on the femto- to picosecond time scales, mainly due to electron-electron and/or electron-phonon interactions,^{3,4} and precludes the use of conventional sources of radiation typically employed for ARPES, e.g., gas-discharge lamps providing continuous-wave radiation, or synchrotron sources offering pulsed beams with duration on the order of 100 ps. In this regard laser-based instruments are particularly suitable for time-resolved ARPES: such systems are capable of delivering pulses of ultrashort (tens of femtoseconds or less) duration and allow for precise synchronization between the pump and probe processes.^{5,6} The short wavelength radiation required for the photoemission process can be achieved through various frequency up-conversion techniques. One possible method is high-harmonic generation (HHG), which provides coherent, ultrashort radiation covering the spectral region from vacuum UV to soft x-rays.^{7,8} Several groups have successfully shown the implementation of HHG in time-resolved photoemission spectroscopy on solids: Haight *et al.*^{5,9} developed this technique to study carrier dynamics at semiconductor surfaces, Quere *et al.*¹⁰ observed energy relaxation in photoexcited quartz, Bauer *et al.*¹¹ and Miaja-Avila *et al.*¹² traced femtosecond surface chemistry reaction

from molecular oxygen and xenon deposited on platinum, respectively, Read *et al.*¹³ studied the decay of excitations on a dye-doped organometallic material, Siffalovic *et al.*¹⁴ traced hot-electron dynamics from platinum surface, and Siffalovic *et al.*¹⁵ and Melzer *et al.*¹⁶ observed transient surface photovoltage in optically excited *p*-GaAs and Ga-covered Si surface, respectively.

In comparison with light sources typically employed in the UV range, which have successfully been used for time-resolved ARPES,^{17–20} the use of high-harmonic radiation extends the information that can be possibly obtained in several ways. (1) HHG, typically in the extreme UV (XUV) range (15–50 eV), allows access to deep, in some cases core-electron levels. (2) The broad energy range covered by HHG offers the possibility to select a particular photon energy which optimizes the photoemission from a given orbital of interest, e.g., *d*- versus *f*-electrons. (3) The use of higher-energy photons extends the accessible momentum space. (4) Optical excitation with sufficiently intense pump pulses introduces a background due to multiphoton photoemission,²¹ which can easily extend beyond the UV range and prevent one from observing the ultrafast dynamics of the transient electrons; the use of XUV photons offers the chance for probing these electrons at energies where the background signal is negligible.¹⁴

Since in HHG a multitude of discrete harmonic peaks is produced, successful utilization of such a source for ARPES experiments requires the spectral selection of a single harmonic order with maximum efficiency while preserving the femtosecond pulse duration. Harmonic selection using a diffraction grating can significantly stretch the pulse in the time domain,²² while the alternative method of using multilayered mirrors^{14,23} offers the convenience of copropagating visible and XUV beams (useful for spatio-temporal overlap between the pump and probe pulses), but lacks convenient wave-

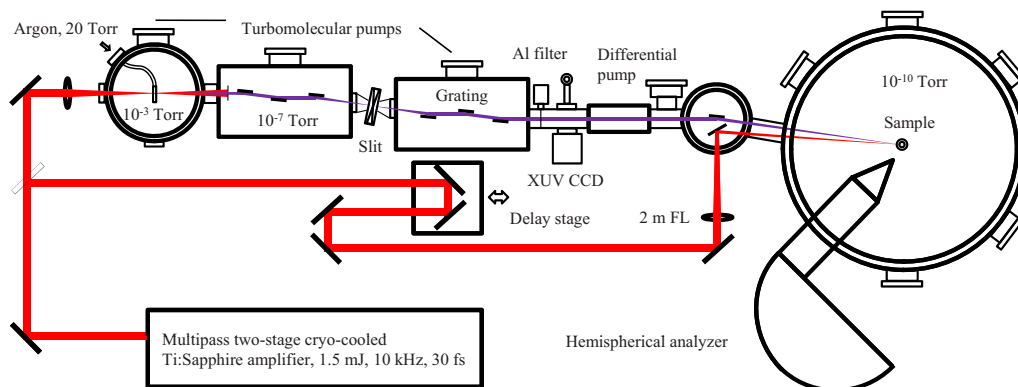


FIG. 1. (Color online) Experimental setup for visible pump/XUV probe ARPES: the visible beam (1.55 or 3.1 eV) traverses a delay stage that controls the timing of the pulses; the XUV beam is produced via HHG in argon, propagates through a TDCM for spectral selection, and is refocused almost collinearly with the visible beam on the sample in a UHV chamber, containing a hemispherical electron analyzer.

length selectivity. Recently Poletto *et al.*^{24,25} proposed and developed a time-delay compensated monochromator (TDCM) that utilizes a pair of diffraction gratings operated in the off-plane mount, demonstrating spectral selection with high efficiency in a broad spectral range²⁶ while preserving the temporal properties of the HHG radiation.²⁷

In this paper we demonstrate the capabilities of a laser-based instrument, employing HHG and a double-grating monochromator (TDCM), together with a highly sensitive hemispherical electron analyzer to obtain static and time-dependent photoemission spectra. We show that single harmonics from a wide energy window, 20–36 eV (for HHG using argon), can be easily selected with the help of the TDCM, and doing so while preserving a high flux of XUV light, $\sim 10^9$ – 10^{10} photons/s per harmonic. We exploit the ability of the detection system to collect two-dimensional images and present angle-resolved photoemission maps of GaAs and URu₂Si₂. Finally, the ability of the apparatus to record time-resolved photoemission is demonstrated by tracing the electron dynamics of optically excited (1.55 eV) single-crystal germanium.

II. EXPERIMENTAL SETUP

A schematic view of the experimental setup is shown in Fig. 1. The laser system is a two-stage Ti:sapphire multipass amplifier (Red Dragon, KMLabs), seeded by a Ti:sapphire oscillator (Halcyon, KMLabs) delivering 6 nJ pulses at ~ 90 MHz repetition rate. The amplification occurs in cryogenically cooled (40 K) crystals pumped by the second harmonic (~ 100 W) of a pair of *Q*-switched Nd:yttrium aluminum garnet lasers (Photonics Industries). The system is capable of routinely delivering 1.5 mJ, 30 fs pulses at 10 kHz repetition rate, with a possible increase up to 20 kHz. The output is split in two arms, with approximately 90% of the energy being used for the process of HHG, and the remaining 10% used to optically excite the samples either at the fundamental (1.55 eV) or the second harmonic (3.1 eV) wavelengths. A single high-order harmonic with ultrashort pulse duration is extracted by passing the XUV beam through a TDCM. The pump and probe beams are focused almost collinearly ($\sim 1^\circ$ angle) onto the sample, positioned in a custom-built ultrahigh vacuum (UHV) chamber. Photo-

emission spectra are acquired with a hemispherical electron analyzer (Specs, Phoibos 150), equipped with a two-dimensional detector for simultaneous energy and momentum detection. In the following sections we will describe in more detail the main components of the apparatus, followed by first applications.

A. XUV light source

HHG is a well-understood process used to convert intense visible or infrared pulses into radiation with a much shorter wavelength. Briefly, in the picture of the three-step model,^{28,29} the interaction of intense ($\sim 10^{14}$ W/cm²) pulses with the atoms of a noble gas leads to ionization, free propagation, during which electrons accumulate energy, and recombination, accompanied by the release of high-energy photons. Due to the inversion symmetry of the generating medium, odd harmonics are produced with energies currently extending up to hundreds of eV, depending on the parameters of the driving pulses and the phase-matching conditions.^{7,8}

We use a 300 mm lens to focus the *s*-polarized laser beam through a 250- μ m-thick LiF window into a vacuum chamber, containing a quasistatic gas cell supplied with argon. The gas cell is formed by a thin-wall nickel tube with a 3 mm diameter, perpendicularly positioned to the direction of the beam. The tube is placed at the focal point and the laser is allowed to drill holes, thus reducing to a minimum the gas load in the chamber. The vacuum chamber is maintained at a pressure of 2×10^{-7} Torr in the absence of gas by using a turbomolecular pump (Varian, 230 l/s). The argon delivery is monitored by a mass-flow controller (MKS); we are capable of increasing the backing pressure inside the tube up to 100 Torr while maintaining a background chamber pressure below 5×10^{-3} Torr. The high-harmonic signal is optimized while observing the beam on an XUV charge-coupled device (CCD) camera (PIXIS-XO, Princeton Instruments). A 500-nm-thick Al filter is placed in front of the camera to reject any stray visible light. Best results are usually obtained when the incident pulse energy is 0.6–0.8 mJ and the argon pressure is 20–30 Torr. The focal point of the laser is

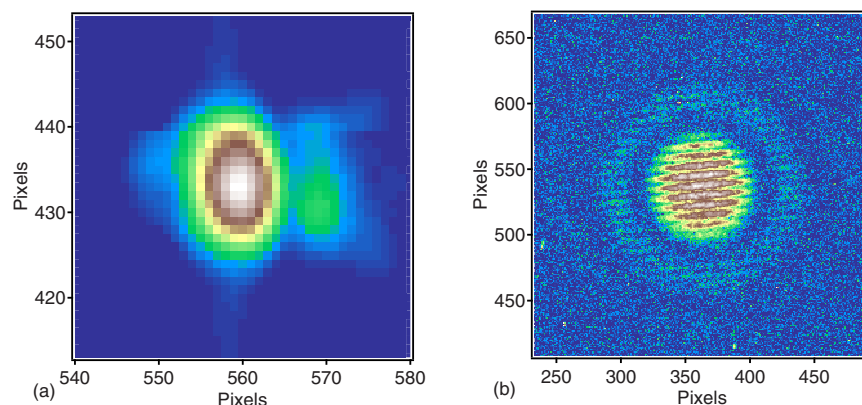


FIG. 2. (Color online) (a) An image of the beam on the CCD camera (1 pixel = $13\ \mu\text{m}$) containing all harmonics. The average size is $120\ \mu\text{m}$ FWHM. (b) Interference pattern of H13 from a double-pinhole ($20\ \mu\text{m}$ in diameter, $100\ \mu\text{m}$ apart). The outer ring results from overlapping diffraction Airy patterns originating from both pinholes.

1–2 mm before the center of the nickel tube and the beam diameter is reduced to 6–8 mm.³⁰ A small aperture (1.5 mm diameter, 20 mm long) at the exit of the chamber allows us to significantly reduce the gas load into the TDCM and subsequent chambers.

A typical image of the XUV beam collimated 300 mm after the HHG source, containing all harmonic orders, is shown in Fig. 2(a). The beam has a nearly Gaussian spatial profile with a size of $\sim 120\ \mu\text{m}$ full width at half maximum (FWHM). We measured the spotsize at two additional positions by translating the camera, and obtained a divergence of less than 0.1 mrad, which is important since the beam is eventually refocused in the target chamber. Since we are observing a polychromatic beam this value represents the divergence of the longest-wavelength component of the beam at a photon energy of $\sim 17\ \text{eV}$, based on the transmission of the Al filter.

We tested the spatial coherence of the XUV beam by observing the interference pattern of H13 (13th harmonic, $\hbar\omega = 20.15\ \text{eV}$) from a pair of $20\ \mu\text{m}$ pinholes, separated by $100\ \mu\text{m}$. The resulting [Fig. 2(b)] fringe visibility of $\sim 80\%$ indicates very good spatial coherence across the diameter of the beam.

In order to characterize the spectral content of the beam, we recorded at room temperature a photoemission spectrum of a Mott-insulator, uranium dioxide (UO_2), using the full spectrum of the XUV beam. The material exhibits a strong, 5- f electron peak with a very small dispersion, less than 1 eV below the Fermi edge, suitable for observing individual harmonic orders (see also Fig. 5). A typical angle-integrated photoelectron spectrum obtained for $\sim 5\ \text{min}$ is shown in Fig. 3. 5- f electron peaks originating from various harmonic orders form a comb structure on top of a background due to photoelectrons with lower kinetic energy. Accounting for the analyzer work function ($\sim 4.2\ \text{eV}$) we get high harmonics up to $\sim 45\ \text{eV}$, which is typical for argon as a generating medium.³¹ As expected the harmonic peaks are spaced by $\sim 3.1\ \text{eV}$, twice the fundamental photon energy, and the width of individual peaks is 0.6–0.8 eV FWHM.

B. Time-delay compensated monochromator

An important requirement for successful utilization of HHG in time-resolved ARPES experiments is the extraction of a single harmonic from the typically broad spectrum, and doing so while preserving the ultrashort duration of the XUV radiation. In addition, it is desirable to be able to select with relative ease the wavelength of choice depending on the particular case of interest, e.g., to maximize photoemission cross-section from a given orbital, or to obtain a bulk versus surface sensitive probe. Recently a TDCM (Ref. 32) has been proposed, built, and thoroughly characterized, demonstrating the ability to fulfill the aforementioned requirements. Briefly, the TDCM is a double-grating monochromator operated in subtractive dispersion mode consisting of two identical sections. The first section contains a collimating mirror, a grating, and a focusing mirror that spectrally disperses the XUV beam, while the second part compensates for the pulse stretching that is inherent in the diffraction process. Wavelength selection is achieved through a simultaneous rotation of the gratings and adjustment of a slit positioned in the intermediate plane between the two sections. One of the most appealing features of TDCM is the excellent throughput, typically in the 10%–15% range. It is attributed to the very high diffraction efficiency (50–70 % at the blaze wave-

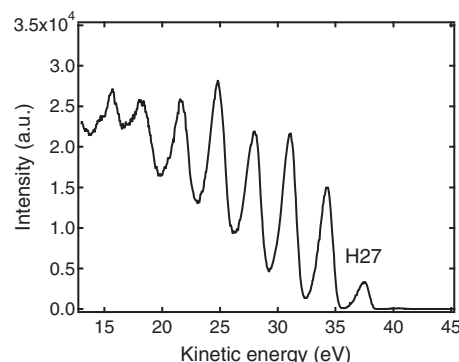


FIG. 3. Photoemission spectrum from UO_2 using a XUV beam containing all generated high-harmonics. The peaks are replicas of the 5- f electronic structure near the Fermi edge, separated by $2\hbar\omega$. Analyzer work function is $\sim 4.2\ \text{eV}$.

length) of the gratings operated at small grazing incidence angle and mounted in the off-plane configuration where the incident and diffracted wave vectors are almost parallel to the grooves of the grating.²⁶ We have adopted a very similar design and constructed a TDCM.

All optical elements in our TDCM are designed and operated at 3° grazing angle. Gold toroidal mirrors ($50 \times 10 \times 10$ mm, ARW Optical) with a 300 mm focal length are used to collimate and refocus the XUV beam while dispersion is achieved using plane-ruled, gold-coated diffraction gratings ($40 \times 40 \times 10$ mm, Richardson Gratings, Newport). Based on the grating equation, and for a given incidence angle, choosing gratings with a particular groove density and blaze angle allows us to operate at a desired wavelength range where the TDCM transmission is maximized, e.g., the efficiency of a 400 g/mm grating blazed at 15° peaks at ~ 18.3 eV. If a significantly longer or shorter wavelength is desired, a straightforward swap of the gratings ensures maximum transmission through the TDCM (provided that the desired wavelength “exists” in the HHG spectrum). All mirror mounts are equipped with a pair of vacuum-compatible actuators (Newport) allowing for a fine beam adjustment while the system is under vacuum. The gratings are positioned on high-precision goniometers (Advanced Design Consulting), allowing for $\pm 10^\circ$ rotation. The slit (Advanced Design Consulting) consists of four tantalum blades that can move independently with a $2 \mu\text{m}$ resolution. The last toroidal mirror in the TDCM has been replaced with a flat mirror, so that a collimated beam would exit the TDCM before it is refocused on the sample in the target chamber. The TDCM is kept under vacuum (2×10^{-7} Torr) with the help of two turbomolecular pumps (Varian, 230 l/s). Overall the TDCM has been designed not as a high resolution apparatus, but rather as a device selecting a single (or multiple, if desired) harmonic order with sufficient bandwidth to support ultrashort pulses necessary for time-resolved photoemission experiments. Nevertheless, the presence of a slit for spectral selection offers some flexibility. For instance, observing the Fermi edge of Pt at 77 K and closing the slit on a single harmonic order, we measure energy resolution of ~ 100 meV with a reasonable flux of XUV photons.

C. Differential pump and UHV target chamber

In order to bridge the difference in pressures in the TDCM and the UHV target chamber, we propagate the XUV beam through a commercially available differential pump (XIA LLC) consisting of a 600 mm long aperture with a square 3×3 mm profile, evacuated by an ion pump. The extremely low gas conductance allows us to maintain undisturbed UHV in the target chamber under operational conditions.

The custom-built UHV chamber is kept at 1×10^{-10} Torr after standard bakeout at 150°C with the help of a turbomolecular (Varian, 500 l/s), an ion (Varian, Starcell), and a titanium sublimation (Varian) pumps. The samples are placed on a copper holder attached to a multidimensional (three translation and one rotation) positioning stage, and cleaved *in situ*. A closed-loop helium cryocooler (Advanced Research Systems) can cool down the samples to

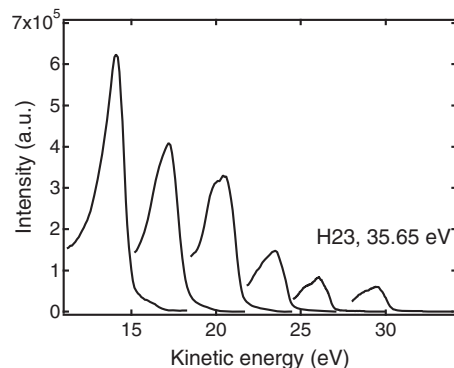


FIG. 4. Photoemission spectra of copper, obtained by selecting individual harmonics. The peaks originate from $3d$ electrons; the small step ~ 2.5 eV above the peak represents the Fermi edge.

12 K. The entrance of the hemispherical electron analyzer forms an angle of 45° with the XUV beam and lies in the same horizontal plane. A load-dock station allows for rapid transfer of samples in the target chamber without breaking vacuum. The chamber is also equipped with an argon sputtering gun (Perkin-Elmer) and a gas-discharge helium lamp (Specs), serving as a well-calibrated source at either He I (21.2 eV) or He II (40.8 eV).

III. PHOTOEMISSION MEASUREMENTS USING SINGLE HARMONICS

We demonstrate the tunability of the apparatus by selecting individual harmonic orders using a pair of gratings with a blaze wavelength at a photon energy of ~ 18.3 eV and collecting for each harmonic photoemission spectra of polycrystalline copper at room temperature. The results are shown in Fig. 4. For each harmonic qualitatively similar features are observed, e.g., for H13 ($\hbar\omega = 20.15$ eV) the “step” at ~ 16.5 eV represents the Fermi edge and the strong peak approximately 2.5 eV below the edge originates from d -electrons. The relative strength of signal between various harmonic orders is a convolution between the efficiency of HHG at the source, the overall transmission of the TDCM, and the energy dependence of the photoemission cross-section. A comparison with measurements performed with He II indicates that for the strongest harmonics we have a flux of $\sim 10^{10}$ photons/s incident on the sample.

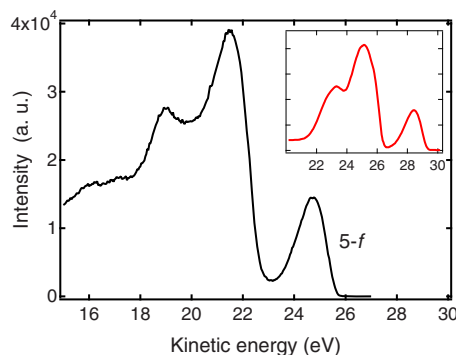


FIG. 5. (Color online) Angle-integrated photoemission of UO_2 using $\hbar\omega = 32.55$ eV. The inset shows the spectrum obtained at SRC (Stoughton, WI) using $\hbar\omega = 34$ eV.

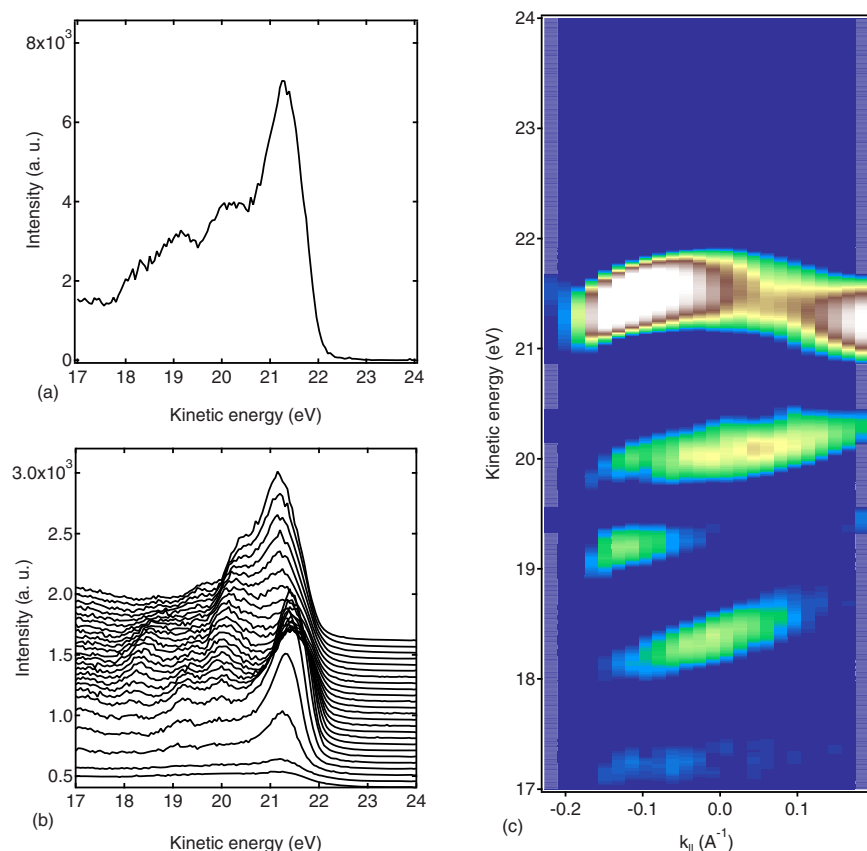


FIG. 6. (Color online) (a) Angle-integrated photoemission from GaAs at 12 K using $\hbar\omega=26.35$ eV. (b) Angle-resolved photoemission at $\pm 4^\circ$ analyzer acceptance angle; the range of accessible momentum values is split in 25 channels. (c) The resulting energy-momentum photoemission map.

A photoemission spectrum of single crystal UO_2 using H21 ($\hbar\omega=32.55$ eV) at room temperature is shown in Fig. 5. The relatively flat electronic bands allow for an angle-integrated collection of data. The acquisition time was ~ 5 min at a pass energy $E_{\text{pass}}=20$ eV and angular acceptance of $\pm 4^\circ$. The inset shows the spectrum obtained at $\hbar\omega=36$ eV using the beamline at the Synchrotron Radiation Center (Stoughton, WI). The two photoemission spectra are in excellent qualitative agreement.

IV. ARPES USING HIGH HARMONICS

Thin GaAs (100) wafers ($500\ \mu\text{m}$) were cleaved at 12 K and photoelectrons emitted from the edge facing the analyzer entrance were recorded using H17 ($\hbar\omega=26.35$ eV). At this photon energy and analyzer acceptance angle of $\pm 4^\circ$, the resulting range of accessible momentum values is $\pm 0.21\ \text{\AA}^{-1}$. Figure 6(a) shows an angle-integrated spectrum, dominated by a strong peak originating from the top of the valence band. Separation of the detected photoelectrons in 25 channels corresponding to different emission angles results in the angle-resolved spectrum shown in Fig. 6(b). The spectrum represents the average of four scans with a total acquisition time of ~ 90 min. The resulting two-dimensional photoemission map is presented in Fig. 6(c). The exact orientation of the exposed surface was not measured, but the appearance of three distinct photoemission peaks indicates that we are probably observing bands dispersing parallel to the Σ direction as reported by Haight *et al.*⁹

As pointed out by Mathias *et al.*²³ the small XUV spot size ensures good momentum resolution, and the main broadening mechanism in ARPES maps obtained using HHG stems from the intrinsic bandwidth of the individual harmonic. Measurement of the Fermi edge of platinum indicates that the FWHM of a single harmonic is typically 400–600 meV (depending on the harmonic order, phase-matching conditions, etc.). Another factor contributing to the broadening comes from the space charge effect. At the estimated photon flux, we expect to have at most 2×10^5 electrons/mm per pulse³³ (for a XUV spot of $200\ \mu\text{m}$ in diameter) and based on a recent investigation,³⁴ a corresponding spectral broadening of about 200 meV, which is in agreement with the spread measured by Mathias *et al.*²³ using a similar XUV source. A possible increase in energy resolution can be achieved by restricting this bandwidth (via the slit in the TDCM), at the expense of lowering the photon flux and increasing the acquisition time.

As another example of ARPES using HHG, we have performed measurements on a heavy-fermion system. The enigmatic hidden-order phase in URu_2Si_2 generates great interest in the solid-state community currently. At least three different energy scales coexist in this compound at very low temperatures. The largest scale is the hybridization gap, already well developed below 50 K. The hidden-order gap, with yet unknown order parameter, forms below 18 K. Finally, the superconducting gap forms at 1.5 K. Our measurement of the electronic structure of URu_2Si_2 shown here in Fig. 7 is the first example of a momentum-resolved disper-

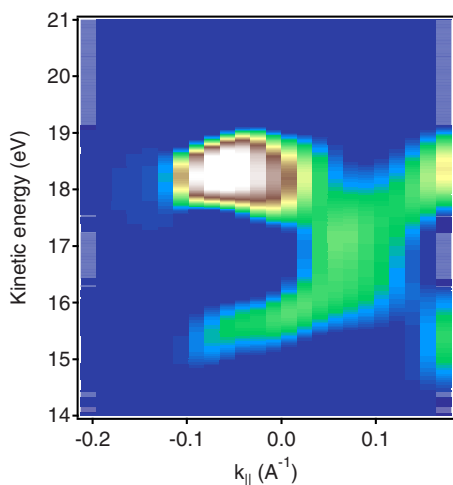


FIG. 7. (Color online) Angle-resolved photoemission map of URu_2Si_2 at 12 K using $\hbar\omega=23.25$ eV.

sive band structure measured in a 5-*f* electron system with a high-harmonic light source. Next, we plan to measure the largest energy scale directly, by using the pump-probe setup and populating the unoccupied part of the hybridization gap.

V. TIME-RESOLVED PHOTOEMISSION

An important prerequisite for the successful observation of time-resolved photoemission using HHG is the correct alignment of the pump and probe beams. Spatial overlap between the two pulses is ensured by observing the fluorescence from both beams on a P43 phosphor screen (Beam Imaging Solutions), positioned on the sample holder and imaged with a CCD camera (DataRay). The size of the XUV and visible pulses is estimated to be 100 and 200 μm FWHM, respectively. As a preliminary step for finding the temporal overlap, the gratings in the TDCM are rotated to zero order to allow the visible beam to propagate through the beamline and the autocorrelation between the visible pulses from the pump and probe arms is measured in a β -barium borate crystal positioned outside the target chamber. The zero delay at the sample position can then be calculated. The actual zero delay between the visible and XUV pulses is very close to this estimate.

Figure 8(a) shows angle-integrated photoemission ($\hbar\omega$

$=26.35$ eV) of single crystal Ge at room temperature at and 30 ps after the arrival of a pump pulse ($\hbar\omega=1.55$ eV) with intensity of 2×10^{11} W/cm², and mixed *s*- and *p*-polarization. The sample surface was oriented perpendicularly to the beam (45° angle between the surface normal and the analyzer entrance) and electrons photoemitted at angles $\pm 14^\circ$ were recorded. The inset shows the photoelectron spectrum recorded with the XUV beam only. In the presence of the pump beam we notice the appearance of an increased spectral weight between approximately 19 and 22 eV, extending above the valence band maximum. We interpret this result as a transient population of surface and/or defect states, known to appear in the band gap region due to surface reconstruction or contamination, and observed for up to hundreds of picoseconds.^{35,36} Photoemission at negative delay (probe pulse arrives before pump) and that with the pump beam blocked were identical, indicating that space charge effect is not responsible for the observed localized change in the spectral weight. The time evolution of the transient feature, traced at different kinetic energies was similar; the temporal behavior of the integrated spectral weight between 19 and 22 eV is shown in Fig. 8(b). The signal decreases exponentially with a time-constant of 21 ± 2 ps. The relatively long signal buildup at negative delay is attributed either to some residual uncertainty in determination of the zero delay, or to possibly different buildup and relaxation carrier dynamics throughout the Brillouin zone, overlapping when observed in an angle-integrated detection mode. This could be investigated by simultaneously doing angle- and time-resolved photoemission spectroscopy.

Various ultrafast processes occur on the femtosecond time scale³ and their dynamics can be accurately monitored if the pulse duration of the pump and probe pulses is well known. Typically pulse duration characterization of HHG radiation in the XUV region is achieved by observing the laser-assisted photoemission (LAPE) from a noble gas;³⁷ the presence of both XUV and “dressing” visible pulses leads to the appearance of sidebands in the photoelectron spectrum, the duration of the sidebands being a measure of the temporal overlap. Recently a similar effect was observed from a carefully prepared metal surface;^{38,39} this may become a useful method for *in situ* XUV pulse characterization in laser-based ARPES experiments. We plan to use surface LAPE for a

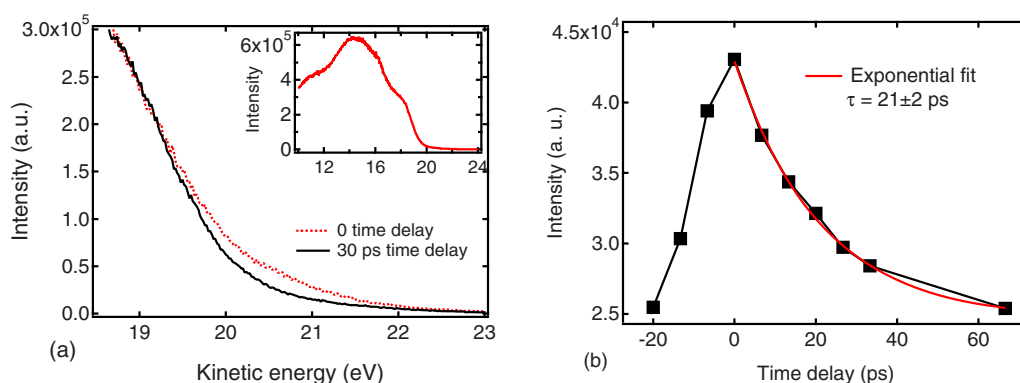


FIG. 8. (Color online) (a) Photoelectron spectra of Ge at time delay of 0 (dotted line) and 30 ps (solid line) between the pump and probe pulses. Pump pulse intensity was $\sim 2 \times 10^{11}$ W/cm². Inset: static photoemission of Ge using $\hbar\omega=26.35$ eV. (b) Dynamics of the transient electron population, integrated in the 19–22 eV kinetic energy range.

more thorough determination of the XUV pulse duration and the ultimate time-resolution of our setup.

VI. CONCLUSIONS AND OUTLOOK

In summary, we presented a table-top laser-based instrument, suitable for static and dynamic ARPES experiments. High-energy photons required for photoemission are produced via HHG in argon, while isolation of a single harmonic order of ultrashort duration is achieved using a time-delay compensated monochromator with excellent throughput. The instrument delivers $\sim 10^{10}$ photons/s per harmonic at a wavelength matching the transmission peak of the gratings. Straightforward wavelength selection via grating rotation and slit adjustment allows for an easy tunability in a wide range of energies. We have demonstrated the capabilities of the apparatus to record angle-resolved photoemission maps, as well as to trace the ultrafast dynamics of transiently occupied optically excited states. Possible applications of this instrument include investigations on ultrafast changes in the electronic structure of high-temperature superconductors, strongly correlated actinide compounds, etc.

ACKNOWLEDGMENTS

Funding for this work is provided by the Laboratory Directed Research and Development Program at Los Alamos National Laboratory under the auspices of the Department of Energy for Los Alamos National Security LLC under Contract No. DE-AC52-06NA25396. We are thankful to Quinn McCulloch (MPA-CINT), Kevin Graham (MPA-CMMS), and Paul Dowden (MPA-STC) for the technical support on this project.

- ¹A. Damascelli, Z. Hussain, and Z. X. Shen, *Rev. Mod. Phys.* **75**, 473 (2003).
- ²Z. X. Shen and D. S. Dessau, *Phys. Rep.* **253**, 1 (1995).
- ³L. Perfetti, P. A. Loukakos, M. Lisowski, U. Bovensiepen, M. Wolf, H. Berger, S. Biermann, and A. Georges, *New J. Phys.* **10**, 053019 (2008).
- ⁴A. Othonos, *J. Appl. Phys.* **83**, 1789 (1998).
- ⁵R. Haight, *Surf. Sci. Rep.* **21**, 275 (1995).
- ⁶M. Bauer, *J. Phys. D: Appl. Phys.* **38**, R253 (2005).
- ⁷A. Rundquist, C. G. Durfee III, Z. Chang, C. Herne, S. Backus, M. M. Murnane, and H. C. Kapteyn, *Science* **280**, 1412 (1998).
- ⁸C. Spielmann, N. H. Burnett, S. Sartania, R. Koppitsch, M. Schnurer, C. Kan, M. Lenzner, P. Wobrauschek, and F. Krausz, *Science* **278**, 661 (1997).
- ⁹R. Haight, J. A. Silbermann, and M. I. Lilie, *Rev. Sci. Instrum.* **59**, 1941 (1988).
- ¹⁰F. Quéré, S. Guizard, Ph. Martin, G. Petite, H. Merdji, B. Carre, J.-F. Hergott, and L. Le Deroff, *Phys. Rev. B* **61**, 9883 (2000).
- ¹¹M. Bauer, C. Lei, K. Read, R. Tobey, J. Gland, M. M. Murnane, and H. C. Kapteyn, *Phys. Rev. Lett.* **87**, 025501 (2001).
- ¹²L. Miaja-Avila, G. Saathoff, S. Mathias, J. Yin, C. La-o-vorakiat, M. Bauer, M. Aeschlimann, M. M. Murnane, and H. C. Kapteyn, *Phys. Rev. Lett.* **101**, 046101 (2008).
- ¹³K. Read, H. S. Karlsson, M. M. Murnane, H. C. Kapteyn, and R. Haight, *J. Appl. Phys.* **90**, 294 (2001).
- ¹⁴P. Siffalovic, M. Drescher, M. Spieweck, T. Wiesenhal, Y. C. Lim, R. Weidner, A. Elizarov, and U. Heinzmann, *Rev. Sci. Instrum.* **72**, 30 (2001).
- ¹⁵P. Siffalovic, M. Drescher, and U. Heinzmann, *Europhys. Lett.* **60**, 924 (2002).
- ¹⁶A. Melzer, D. Kampa, J. Wang, and T. Fauster, *Phys. Rev. B* **80**, 205424 (2009).
- ¹⁷M. Lisowski, P. A. Loukakos, U. Bovensiepen, J. Stahler, C. Gahl, and M. Wolf, *Appl. Phys. A: Mater. Sci. Process.* **78**, 165 (2004).
- ¹⁸L. Perfetti, P. A. Loukakos, M. Lisowski, U. Bovensiepen, H. Berger, S. Biermann, P. S. Cornaglia, A. Georges, and M. Wolf, *Phys. Rev. Lett.* **97**, 067402 (2006).
- ¹⁹F. Schmitt, P. S. Kirchmann, U. Bovensiepen, R. G. Moore, L. Rettig, M. Krenz, J.-H. Chu, N. Ru, L. Perfetti, and D. H. Lu, *Science* **321**, 1649 (2008).
- ²⁰S. Mathias, M. Wiesenmeyer, F. Deicke, A. Ruffing, L. Miaja-Avila, M. Murnane, H. C. Kapteyn, M. Bauer, and M. Aeschlimann, *J. Phys.: Conf. Ser.* **148**, 012042 (2009).
- ²¹M. Aeschlimann, C. A. Schmuttenmaer, H. E. Elsayed-Ali, R. J. D. Miller, J. Cao, Y. Gao, and D. A. Mantell, *J. Chem. Phys.* **102**, 8606 (1995).
- ²²P. Villorresi, *Appl. Opt.* **38**, 6040 (1999).
- ²³S. Mathias, L. Miaja-Avila, M. M. Murnane, H. C. Kapteyn, M. Aeschlimann, and M. Bauer, *Rev. Sci. Instrum.* **78**, 083105 (2007).
- ²⁴L. Poletto and P. Villorresi, *Appl. Opt.* **45**, 8577 (2006).
- ²⁵L. Poletto, P. Villorresi, E. Benedetti, F. Ferrari, S. Stagira, G. Sansone, and M. Nisoli, *J. Opt. Soc. Am. B* **25**, B44 (2008).
- ²⁶M. Pascolini, S. Bonora, A. Giglia, N. Mahne, S. Nannarone, and L. Poletto, *Appl. Opt.* **45**, 3253 (2006).
- ²⁷L. Poletto, P. Villorresi, E. Benedetti, F. Ferrari, S. Stagira, G. Sansone, and M. Nisoli, *Opt. Lett.* **32**, 2897 (2007).
- ²⁸P. Corkum, *Phys. Rev. Lett.* **71**, 1994 (1993).
- ²⁹K. J. Schafer, B. Yang, L. F. DiMauro, and K. C. Kulander, *Phys. Rev. Lett.* **70**, 1599 (1993).
- ³⁰S. Kazamias, F. Weihe, D. Douillet, C. Valentin, T. Planchon, S. Sebban, G. Grillon, F. Auge, D. Hulin, and Ph. Balcou, *Eur. Phys. J. D* **21**, 353 (2002).
- ³¹T. Brabec and F. Krausz, *Rev. Mod. Phys.* **72**, 545 (2000).
- ³²L. Poletto, P. Villorresi, F. Frassetto, F. Calegari, F. Ferrari, M. Lucchini, G. Sansone, and M. Nisoli, *Rev. Sci. Instrum.* **80**, 123109 (2009).
- ³³X. J. Zhou, B. Wannberg, W. L. Yang, V. Brouet, Z. Sun, J. F. Douglas, D. Dessau, Z. Hussain, and Z.-X. Shen, *J. Electron Spectrosc. Relat. Phenom.* **142**, 27 (2005).
- ³⁴S. Hellmann, K. Rossnagel, M. Marczyński-Bühlöw, and L. Kipp, *Phys. Rev. B* **79**, 035402 (2009).
- ³⁵J. Bokor, R. Haight, J. Stark, R. R. Freeman, and P. H. Bucksbaum, *Phys. Rev. B* **32**, 3669 (1985).
- ³⁶R. Haight, J. Bokor, R. R. Freeman, and P. H. Bucksbaum, *J. Vac. Sci. Technol. A* **4**, 1481 (1986).
- ³⁷T. E. Glover, R. W. Schoenlein, A. H. Chin, and C. V. Shank, *Phys. Rev. Lett.* **76**, 2468 (1996).
- ³⁸L. Miaja-Avila, C. Lei, M. Aeschlimann, J. L. Gland, M. M. Murnane, H. C. Kapteyn, and G. Saathoff, *Phys. Rev. Lett.* **97**, 113604 (2006).
- ³⁹G. Saathoff, L. Miaja-Avila, M. Aeschlimann, M. M. Murnane, and H. C. Kapteyn, *Phys. Rev. A* **77**, 022903 (2008).